Published online 29 September 2006 *Nucleic Acids Research, 2006, Vol. 34, No. 19* ***5361–5368***
doi:10.1093/nar/gkl580

Molecular dynamics simulations of human $tRNA^{Lys,3}_{UUU}$: the role of modified bases in mRNA recognition

Nina E. McCrate, Mychel E. Varner, Kenneth I. Kim and Maria C. Nagan*

Division of Science, Truman State University, 100 East Normal, Kirksville, MO 63501, USA

Received May 18, 2006; Revised July 21, 2006; Accepted July 24, 2006

ABSTRACT

Accuracy in translation of the genetic code into proteins depends upon correct tRNA–mRNA recognition in the context of the ribosome. In human $tRNA^{Lys,3}_{UUU}$ three modified bases are present in the anticodon stem–loop—2-methylthio-*N*6-threonylcarbamoyladenosine at position 37 (ms^2t^6A37), 5-methoxycarbonylmethyl-2-thiouridine at position 34 (mcm^5s^2U34) and pseudouridine (ψ) at position 39—two of which, ms^2t^6A37 and mcm^5s^2U34, are required to achieve wild-type binding activity of wild-type human $tRNA^{Lys,3}_{UUU}$ [C. Yarian, M. Marszalek, E. Sochacka, A. Malkiewicz, R. Guenther, A. Miskiewicz and P. F. Agris (2000) *Biochemistry*, 39, 13390–13395]. Molecular dynamics simulations of nine tRNA anticodon stem–loops with different combinations of nonstandard bases were performed. The wild-type simulation exhibited a canonical anticodon stair-stepped conformation. The ms^2t^6 modification at position 37 is required for maintenance of this structure and reduces solvent accessibility of U36. Ms^2t^6A37 generally hydrogen bonds across the loop and may prevent U36 from rotating into solution. A water molecule does coordinate to ψ39 most of the simulation time but weakly, as most of the residence lifetimes are <40 ps.

INTRODUCTION

Nonstandard bases are most prevalently found in tRNA molecules and may involve a variety of modifications from simple methylation to addition of a peptide moiety (1,2). Some tRNA molecules require posttranscriptionally modified nucleic acid bases for proper translation (3,4), recognition by proteins (5,6) and initiation of human immunodeficiency virus reverse transcription (7). Specifically, ribosomal binding (8,9), proper translocation from the aminoacyl site (A) to peptidyl site (P site) (10,11) and translational speed (12) may be dependent upon nonstandard bases, while the lack of modified bases may result in frameshifting errors (13). Most tRNAs contain at least one modified base (14) and modifications often occur at positions 34 and 37 (4). Modified bases are generally thought to increase stability of tRNA structure by providing additional hydrogen-bonding contacts, better base–base stacking interactions (4,15–19) and metal ion binding sites (20–22). Specifically, base modifications at the 34th and 37th positions of the tRNA are often important for facilitating cognate codon recognition (4). Still, the role specific modifications play in determining RNA structure, stability and function are not well understood.

Functional groups in modified nucleosides can dramatically affect the ability of tRNA anticodons to recognize their cognate mRNA codon and therefore participate in accurate translation of the genetic code (15,16). The third human tRNA coding for lysine ($tRNA^{Lys,3}$) contains three posttranscriptionally modified bases in the anticodon stem–loop (ASL, Figure 1). Biochemical assays have established that 5-methoxycarbonylmethyl-2-thiouridine at position 34 (mcm^3s^2U34) and 2-methylthio-*N*6-threonylcarbamoyl-adenosine at position 37 (ms^2t^6A37) are required to mimic wild-type human $tRNA^{Lys,3}$ binding to programmed ribosomes (9). Pseudouridine (ψ) presence at position 39 is not critical to anticodon–codon recognition but has been shown to contribute to helical stability (17). *Escherichia coli* $tRNA^{Lys,}$, analogous to its human counterpart, contains a 5-methylaminomethyluridine-2-thiouridine at position 34 (mnm^5s^2U34) and *N*6-threonylcarbamoyl-adenosine at position 37 (t^6A37) that are both important for ribosomal A site binding (8,9,23), translocation from the A site (11) and discrimination between AAA and AAG codons (24,25).

Several structures of human $tRNA^{Lys,3}$ and *E.coli* $tRNA^{Lys}$, variants with variously modified bases in a variety of contexts have been determined by both NMR spectroscopy (18,26–29) and X-ray crystallography (19,30). The expensive and often complex synthesis of nonstandard bases further complicates incorporation of all fully modified bases. Structural studies indicate that preservation of a U-turn motif in *E.coli* anticodon loop is important for recognition of cognate mRNA (28). Systematic, detailed NMR studies of fully modified *E.coli* and partially modified human $tRNA^{Lys,3}$ indicate flexibility in the U36 position (29). In the context of the 30S ribosomal subunit, an anticodon loop containing t^6A37 has been found to recognize the cognate mRNA codon (19) in a canonical Fuller–Hodgson tRNA form (31).

*To whom correspondence should be addressed. Tel: +1 660 785 4084; Fax: +1 660 785 4045; Email: mnagan@truman.edu

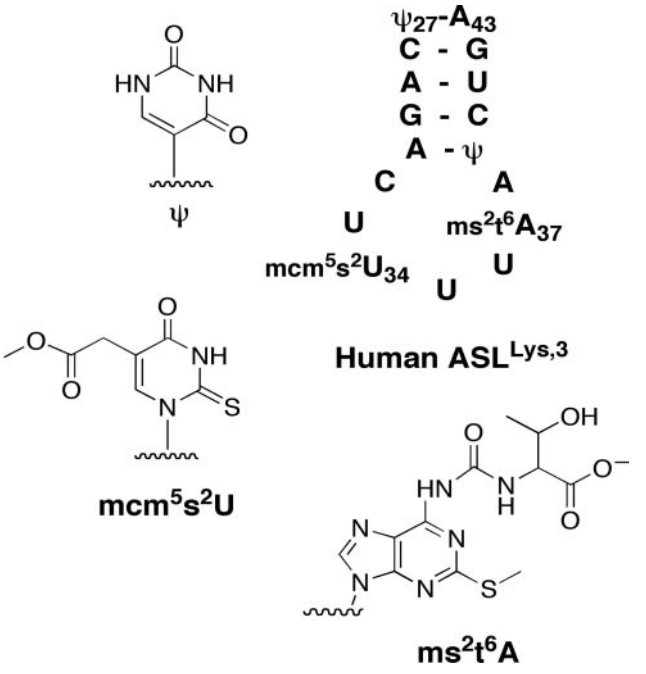

Figure 1. Secondary structure of human $tRNA^{Lys,3}$ ASL. Chemical structures of modified bases found in $ASL^{Lys,3}$.

The contributions of each modified base to free tRNA and ribosomally bound tRNA structures remains elusive (4,16,32). Molecular dynamics (MD) studies considering specific contributions of modified bases mcm^5s^2U34, ms^2t^6A37, ψ39 to the structure and function of the human $ASL^{Lys,3}$ are reported. Specifically, the role of modified bases in preserving canonical tRNA anticodon structure is examined.

METHODS

Initial structures

Fully refined NMR structures are currently not available for fully modified $tRNA^{Lys,3}$; therefore all simulations were begun from X-ray crystal structures. MD simulations of the $tRNA^{Lys,3}_{UUU}$ anticodon stem–loop with bases 27–43 ($ASL^{Lys,3}$ wild type) derived from the fully modified $tRNA^{Lys,3}$ X-ray crystal structure solved to 3.3 Å resolution (PDB code 1FIR) (30) were performed with different combinations of mcm^5s^2U34, ms^2t^6A37, ψ39 and unmodified bases (Table 1). All variations of $ASL^{Lys,3}$ were derived from the Bénas *et al.* (30) structure. While this study was being conducted, the crystal structure of *E.coli* $ASL^{Lys,}$, which contains t^6A37, with the 30S ribosomal subunit and mRNA was solved to 3.0 Å resolution (PDB code 1XMQ) (19). In *E.coli* $ASL^{Lys,}$, the ureido ring of t^6A37 stacks with A38 stabilizing anticodon–codon interactions. To ensure adequate sampling of relevant structures, an additional system, wild-type 2, was derived by grafting the *E.coli* $ASL^{Lys,}$ anticodon loop containing an ureido ring in t^6A onto the Bénas $ASL^{Lys,3}$ stem and applying the appropriate full-human $ASL^{Lys,3}$ modifications.

Molecular dynamics simulations

All MD simulations were performed according to the same protocol. Trajectories were propagated with the Cornell *et al.* force field (33), as implemented in the SANDER module of the program AMBER 6.0 (34). ASLs were solvated by a 10 Å rectangular box of TIP3P water (35) and Na^+ ions were added to neutralize the system. Simulations were performed under periodic boundary conditions, employing the particle mesh Ewald (36) formalism to account for long range electrostatics.

MD trajectories were propagated with a 2.0 fs time step, employing the SHAKE algorithm (37) on all hydrogen atoms, with a nonbonded cutoff of 9.0 Å. The pairlist was updated every 25 steps. Constant pressure (1 atm) and temperature (300 K) were maintained according to the Berendsen coupling algorithm (38). The equilibration protocol of Cheatham was followed (39) similar to previous simulations of nucleic acids (40–45). Simulations were allowed to equilibrate under production-run conditions for at least 2.0 ns before collection of statistics over 4.0 ns.

Table 1. The role of ms^2t^6A37

$ASL^{Lys,3}$	% Stair-stepped	SASA ($Å^2$)
wild-type $ASL^{Lys,3}$—mcm^5s^2U34, ms^2t^6A37, ψ39	96	150 (10)
wild type 2—mcm^5s^2U34, ms^2t^6A37, ψ39	46	140 (20)
$ASL^{Lys,3}$—mcm^5s^2U34, ms^2t^6A37	76	160 (20)
$ASL^{Lys,3}$—ms^2t^6A37, ψ39	99	180 (20)
$ASL^{Lys,3}$—ms^2t^6A37	93	160 (10)
$ASL^{Lys,3}$—mcm^5s^2U34, ψ39	0	230 (30)
$ASL^{Lys,3}$—mcm^5s^2U34	7	230 (10)
$ASL^{Lys,3}$—ψ39	0	250 (10)
$ASL^{Lys,3}$—unmodified	0	250 (10)

Percentage of the simulation anticodons exhibited the stair-stepped conformation (left). SASA for the U36 base (right). Modified bases included in each simulation are indicated. Absence of a modification indicates the unmodified base was substituted at that position.

Force-field parameters

Parameters for nonstandard bases were derived to be consistent with the Cornell *et al.* force field (33) and specific parameters are available in Supplementary Data. Atom types, force constants and equilibrium values were assigned by analogy to the Cornell *et al.* nucleic acid, threonine side chain (t^6) or methionine (ms^2) force-field parameters (33), or the General Amber Force Field (46) for sulfur-related parameters. Partial atomic charges were derived from Hartree–Fock (47)/6-31G* (48–50) electrostatic potential charges fitted with a two-step restrained electrostatic potential procedure (51). Electronic structure calculations were performed with Gaussian 03M, revision B.04 (52).

Ms^2t^6A rotational barrier

Quantum mechanical calculations employing the modified Perdew-Wang 1-parameter model for kinetics (MPW1K) (53,54) and the 6-31+G (d,p) basis set (55,56) were used to determine the rotational barrier around the C10-N11 amide bond involved in ureido ring formation.

Data analysis

Trajectories were analyzed using the CARNAL and PTRAJ modules of AMBER 6.0 (34). All statistics were collected

on 1 ps snapshots over 4.0 ns of data. Helical parameters were measured using the 3DNA program (57). Trajectories and structures were visualized using VMD (58) and UCSF chimera (59). Criteria for hydrogen bonding was a 3.5 Å distance between heavy atoms and a heavy atom-H-heavy atom angle of 180° ± 60°. Solvent accessible surface area (SASA) was calculated as a Connolly surface (60), as implemented in the MM-PBSA module of AMBER 8.0 (61). When determining if bases were parallel, the angle between normal vectors to the plane of the respective bases was used. Planes were defined using three points; N1, N3 and C5 for pyrimidines and N3, C6 and C8 for purines and the normal vectors were defined to point in the 3′ direction.

RESULTS

Trajectories

Trajectory stability was based upon steady fluctuations around constant values for root mean square deviation (r.m.s.d.) values from the average (Figure 2) and starting structures (Supplementary Data) as well as monitoring of helical parameters of the double-stranded region such as local twist, *x*-displacement from the helical axis and base pair inclination (Supplementary Data).

Overall, the helical portion of all ASL structures exhibited classic A-form geometry (62) with *x*-displacement values ranging from −4.5 ± 0.6 to −5.3 ± 0.9 Å and base pair rise parameters of 2.5 ± 0.3 to 2.8 ± 0.3 Å. The majority of structural analysis occurred in the loop region of the ASLs.

The wild-type simulation was unusually stable with an average r.m.s.d. from the starting structure of only 1.8 ± 0.3 Å. To ensure that the wild-type simulation was indeed naturally stable and that periodic effects or lack of sampling time did not influence the results, data for two additional simulations were collected (N. E. McCrate, unpublished data). In the first simulation, the water box surrounding the RNA was increased to 15 Å beyond the solute. In the other simulation, with 10 Å of water added beyond the solute, data were collected for 40 ns. Both additional simulations retained the structure observed in the reported wild-type simulation.

Presence of mcm^{5}s^{2}U34 and/or ms^{2}t^{6}A37 widens the loop region

All simulations contained a hydrogen bond between C32 O2 or N3 and the A38 exocyclic amine to varying extents of the simulation but averaging 74% occupancy. Simulations containing no modified bases or only ψ39, exhibited an additional hydrogen bond between the exocyclic amine of A37 and the O2 of U33 56 and 62% of the simulations time, respectively. Addition of either mcm^{5}s^{2}U34 and/or ms^{2}t^{6}A37 decreased the A37–U33 interaction to <4% of the simulation time.

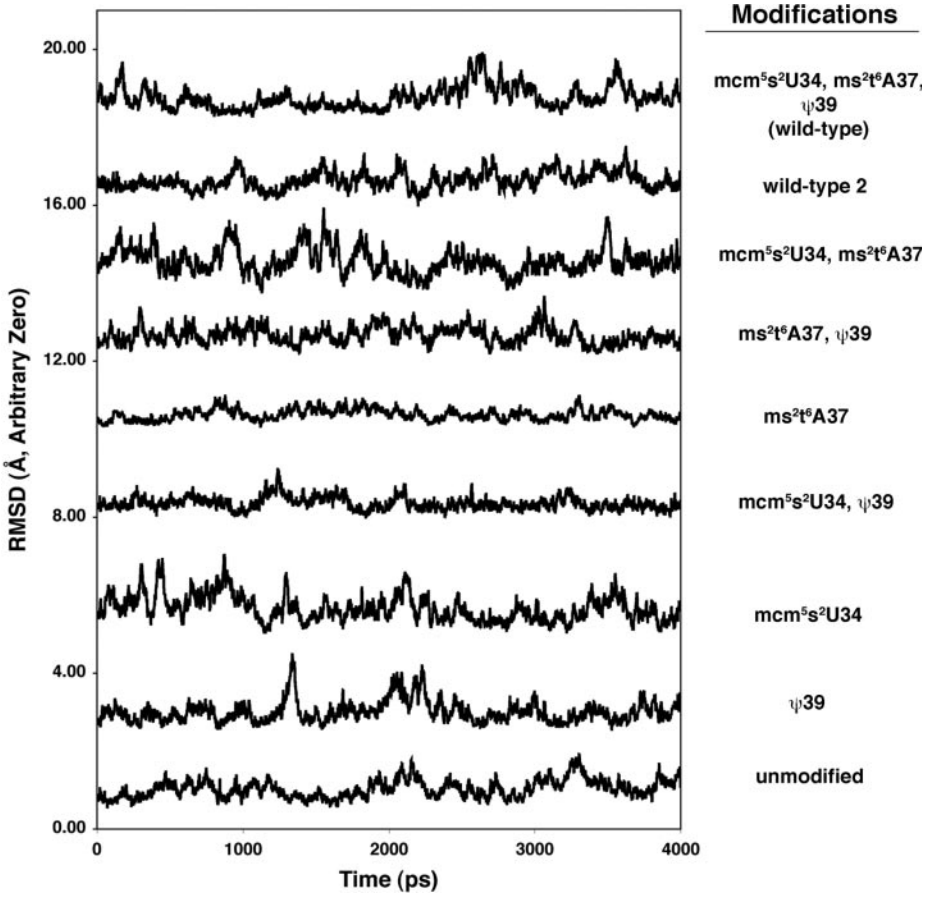

Figure 2. Plots of r.m.s.d. from the average structures. For each simulation, the average structure was calculated solely for the production run. The r.m.s.d. values have an arbitrary zero.

The side chain of mcm^{5}s^{2}U34 did not form hydrogen bonds often with other parts of the ASL. The only detectable hydrogen bond observed occurred between the mcm^5 carbonyl oxygen and the hydroxyl of ms^{2}t^{6}A37 in the wild-type simulation and the simulation containing both mcm^{5}s^{2}U34 and ms^{2}t^{6}A37 for <20% of the simulation time.

In the models presented herein there seems to be no correlation between presence of a U33 NH3 hydrogen bond to U36 O2P and any one conformation. Simulations containing mcm^{5}s^{2}U34 seem to lose a U33 NH3 hydrogen bond with U36 O2P (<3%) while simulations lacking a modification at position 34 close to form this hydrogen bond >90% of the simulation time. The exceptions to this trend are both wild-type simulations, which contain this hydrogen bond 100 and 91% for wild-type and wild-type 2 simulations, respectively.

Characterization of the anticodon stair-step

In the fully modified ASL structure including mcm^{5}s^{2}U34, ms^{2}t^{6}A37 and ψ39 (wild-type ASL^{Lys,3}), the structure retained a stair-stepped conformation, in which the uridines (Figure 3) are offset and nearly parallel to each other, observed previously in the X-ray crystal structures of free human tRNA^{Lys,3} (30) and when *E.coli* t^{6}A ASL^{Lys,} pairs with its cognate mRNA codon in the context of the ribosome (19).

To characterize the stair-stepped conformation, the relative positions of the anticodon bases to each other were determined. To analyze the positions of the anticodon bases relative to each other, the distances between the center of mass (COM) of anticodon bases' aromatic rings were measured. The distance vectors were transformed into a relative coordinate system utilizing a rotation matrix and decomposed into *x* (dx), *y* (dy) and *z* (dz) components, to describe the relative positions of the bases. By analogy, the dx, dy and dz components describe the height width and length of 'the stair'. From visual inspection, the wild-type simulation was determined to exhibit the prototypical stair-stepped conformation. To determine whether the geometry of the anticodon for each model matched that of the wild-type, dx, dy and dz between each set of rings (U34–U35 and U35–U36) were classified as 'stair stepped' if the values for both pairs of rings fell within 4 SDs of the average values calculated for the wild-type model and the angle between the normal vectors of the planes of the bases was 0 ± 45° (63) (Table 1).

To aid in data analysis, snapshots of each simulation were assessed for presence of a stair-stepped conformation. Based upon the criteria outlined above, the percent occupancies of stair-stepped interactions for positions 34–36 were determined (Table 2). Simulations that contained an ms^{2}t^6 modification at position 37 exhibited the stair-stepped anticodon configuration 75–100% of the simulation time, while those ASLs lacking base modifications at position 37 were not stair-stepped for most, if not all, of the simulation. In the wild-type 2 model, in which the anticodon appears to be stair-stepped, the U36 base is positioned closer to the N9 of ms^{2}t^{6}A37 than is observed in the other models. As a result of this difference in position, the wild-type 2 simulation is classified as having a less stair-stepped codon (46%) than the other models because it is stair-stepped in a slightly different conformation.

When ms^{2}t^{6}A37 is substituted with A37, U36 rotates around the glycosidic bond and is exposed to solvent. This

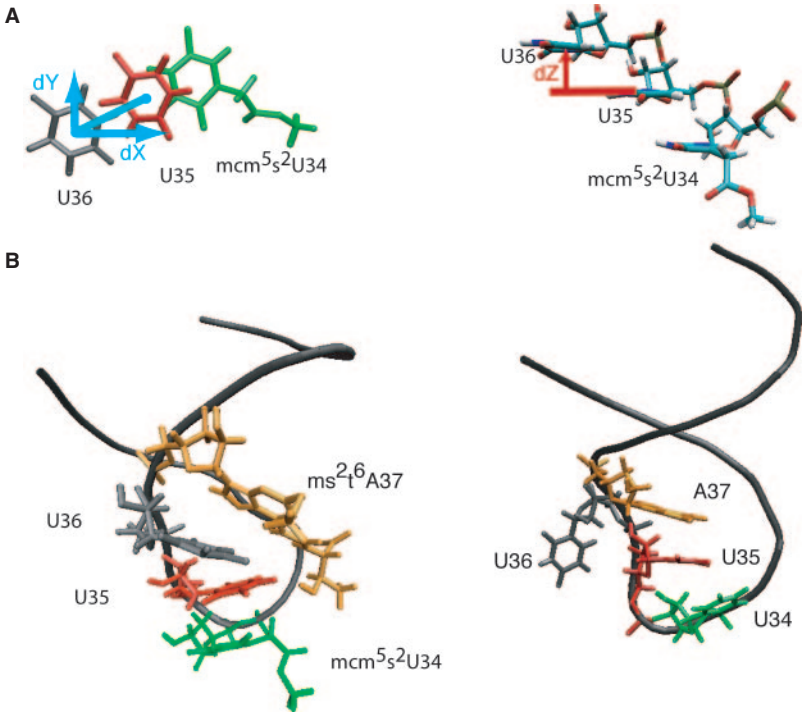

Figure 3. Stair-stepped conformation. (**A**) Stair-stepped conformation of the anticodon bases from the side (left) and from above (right) with dx, dy and dz parameters shown. (**B**) Snapshot of the wild-type simulation showing ms^{2}t^{6}A37 hydrogen bonding across the loop (left) and a snapshot of the ASL^{Lys,3} ψ39 simulation when U36 is rotated into solution (right).

Table 2. Base–base stacking interactions

$ASL^{Lys,3}$	U36–A37 (5)	A37(5)–A38(5)	A37(6)–A38(5)	A37(u)–A38(6)
wild-type $ASL^{Lys,3}$ (mcm^5s^2U34, ms^2t^6A37, ψ39)	34	16	85	
wild-type 2 (mcm^5s^2U34, ms^2t^6A37, ψ39)	21	25	33	67
$ASL^{Lys,3}$—mcm^5s^2U34, ms^2t^6A37	3	85	31	
$ASL^{Lys,3}$—ms^2t^6A37, ψ39	18	33	24	
$ASL^{Lys,3}$—ms^2t^6A37	28	67	32	
$ASL^{Lys,3}$—mcm^5s^2U34, ψ39	1	21	83	
$ASL^{Lys,3}$—mcm^5s^2U34	0	0	0	
$ASL^{Lys,3}$—ψ39	0	16	96	
$ASL^{Lys,3}$—unmodified	0	25	95	

The percent of the simulation time, base stacking was present for interactions between bases U36, A37 and A38 are shown. COM distances between bases were determined for the aromatic rings indicated; 5 indicates the 5-membered ring of A, 6 indicates the 6-membered ring of A and u indicates the ureido ring of ms^2t^6A37. Modified bases included in each simulation are indicated. Absence of a modification indicates the unmodified base was substituted at that position.

was observed in all simulations lacking ms^2t^6 modifications at position 37. Quantification of U36 solvent exposure through the SASA of the U36 base indicates that the presence of the ms^2t^6 modification at position 37 reduces the SASA of U36 (Table 2). Relatively smaller U36 SASA values correspond to the stair-stepped conformation, while larger SASA values correspond to U36 unstacking. In addition, mcm^5s^2U at position 34 appears to slightly lower the SASA of U36 as all models lacking mcm^5s^2 modifications have slightly higher U36 SASA than their modified counterparts (10–30 $Å^2$, Table 1).

Base stacking analysis in the anticodon loop

From visual inspection of the wild-type simulations, it seemed that bases 36–38 were interacting, perhaps by base–base stacking interactions. All simulations were examined to determine the extent of base–base stacking in the anticodon loop. A stacking interaction was defined to occur when the distance measured from the COM between two aromatic rings was <4 Å and the angle between the normal vectors of planes formed by the bases was ±20°, as determined appropriate by previous studies (63,64).

Based on the stacking criteria outlined above, the percent occupancy of stacking interactions for positions 36–38 was determined (Table 2). In all simulations containing ms^2t^6A37, for a portion of the simulation (3–34%), U36 was in close proximity to the A37 5-membered ring. The stacking data indicate that the presence of ms^2t^6A37 may slightly enhance base–base stacking between U36 and position 37.

Ms^2t^6A side chains

Modification of A37 encourages the base to remain intercalated between A38 and U36. In general, A37, modified or unmodified, hydrogen bonds with functional groups in the anticodon loop. Simulations containing ms^2t^6A37 tended to interact across the loop with base and sugar atoms in residues 32–35 for relatively short lifetimes. For instance, in the wild-type trajectory, the hydroxyl group from t^6 was hydrogen bonded for most of the simulation time to some group in the tRNA. It preferred to interact with sugar oxygens in residue 33 but also hydrogen bonded with base oxygens in U34 and U35 carbonyls. When ms^2t^6 modifications were removed, the A37 disrupted the U36–U35 interaction and formed new h-bonds through N6 with bases in closer proximity, such as residues U35, U36 and A38. In the absence of ms^2t^6, the ASL rearranges to provide new hydrogen-bonding partners for the truncated N6 position of A37.

In the context of the ribosome, *E.coli* t^6A37 contains an ureido ring which stacks with the 6-membered ring of A38 (19). The crystal structure of t^6A alone contains an ureido ring (65). In the fully refined $tRNA^{Lys3}$ X-ray structure (PDB code 1FIR), ms^2t^6A37 seems to adopt a conformation without an ureido ring although initial attempts were to try to have a clearer electron density showing an ureido ring-like conformation [P. Bénas, personal communication and figures in Ref. (30)]. Quantum mechanical calculations on *N9*-methylated ms^2t^6A at the MPW1K/6-31+G (d,p) level of theory indicate that the barrier to rotation around the C10-N11 bond to form an ureido ring is ~9.0 kcal/mol at room temperature.

Pseudouridine stabilization

When ψ39 is present, a water bridge forms between A38 O2P, ψ39 NH3 and ψ39 O1P. Although the full water bridge is only present for ~30% of the production run (detailed tables in Supplementary Data), the component hydrogen bonds between ψ39 NH3-water-A38 O2P and ψ39 NH3-water-ψ39 O1P are present for larger percentages of the production run, typically 50–80%. The waters involved in the water bridge are short lived with the bulk of the bridging interaction being attributable to water molecules having lifetimes at or below 40 ps and nearly all residence lifetimes being attributable to waters with lifetimes ⩽120 ps.

DISCUSSION

As has been observed in the *E.coli* $tRNA^{Phe}$ ASL (66) and various studies involving $tRNA^{Lys,}$ variants (18,26,28,29), modifications act sterically in the anticodon loop to widen the loop and prevent a closed structure. This is consistent with the previously observed closed-loop conformation observed experimentally by NMR spectroscopy (18,29). Addition of mcm^5s^2U at position 34 and/or ms^2t^6A at position 37 introduces enough steric hindrance that the loop widens and interactions between U33 and A37 are no longer observed.

Pseudouridine and water

MD simulations with the Cornell *et al*. force field (33) and TIP3P (35) water have been shown to identify long-lived, structural water molecules in other systems (41,44). The water molecule that coordinates with ψ39 is present most of the time but is not long lived. Pseudouridine has been shown to stabilize tRNA structure through a water-mediated hydrogen-bonding network (67). The crystal structure of yeast $tRNA^{Phe}$, which contains a ψ55, has a water molecule bridging the N1-H position to the neighboring phosphate oxygens of T54 and ψ55 (68). Additionally, a long-lived water molecule coordinated to ψ has been found in $tRNA^{Asp}$

through MDs simulations (41). This water-mediated hydrogen bond with ψ is believed to restrict ψ motion and stabilize A–ψ base pairs (41,69,70), which are most prevalently found at positions 31–39 (14).

Canonical tRNA

Overall the wild-type simulation retained the stair-stepped conformation with dx, dy and dz values all similar to that found in the X-ray crystal structure of human $tRNA^{Lys,3}$ (30) and *E.coli* t^6A-ASL bound in the 30S ribosome (19). Modifications at position 37 stabilize the anticodon conformation. From this data it appears that the presence of ms^2t^6A37 encourages retention of a highly ordered stair-stepped conformation.

Base modifications at position 37 seem to stabilize U36 participation in the stair-stepped conformation. U36 is the first base of the anticodon and is required for proper reading of the cognate codon base. The ms^2t^6A37 base is required for proper positioning of U36 to recognize its cognate codon base. Uridine with its hydrophilic carbonyls and N3, in general, is predisposed to an extra-helical position resulting in an increase in solvent exposure as noted in a systematic study of RNAs containing a single-base bulge (71). The highly ordered stair-stepped conformation of the anticodon bases seems to be important to codon recognition as originally hypothesized (31) and observed in crystal structures of tRNAs alone (72), interacting with other tRNAs through crystal packing effects (30,73–75), and in the context of the ribosome (19,76).

Base–base stacking data indicate that modifications on A37 may position the base to better interact with U36. However, this stacking interaction is not long lived in simulations. In order to have favorable base–base stacking interactions, the interaction of two hydrophobic bases must be enthalpically favorable (77,78). In this case, the negative electron densities of the aromatic bases may repel each other and electrostatic interactions, in which positive portions of the base above are interacting with the negative electron density of the base below, may predominate. This favorable electrostatic interaction has been observed in simple systems, such as benzene and water. In these benzene–water pairs, the partially positive hydrogens of the water molecules are interacting with the negative π-cloud of the benzene ring (79). It may be more favorable for a canonical anticodon to be stair-stepped because the positive portions of bases are aligned to interact with the negative π-cloud of the neighboring, lower base. When A37 is modified, it can partake in hydrogen bonds across the anticodon loop, effectively holding it up above U36. When modifications are removed, the base no longer has enthalpically favorable hydrogen-bonding interactions unless U36 rotates into solution, leaving unmodified A37 to favorably interact with U35 through electrostatic interactions and hydrogen bond with closer bases through its truncated 6-amino group.

Conformation of ms^2t^6A

The bulky ms^2t^6 modification containing hydrogen bond donors and acceptors may act sterically to restrict A37 movement while discouraging the displacement of U36 through weak stacking interactions and stabilizing the position of A37 through hydrogen bond contacts across the loop. In the wild-type 2 simulation, where the bulk of the t^6A substituent's hydrogen bond donors and acceptors are solvent exposed, U36 exhibits markedly increased conformational freedom. This behavior suggests a delicate balance of forces, of which cross-strand hydrogen bonding is a portion, preventing the displacement of U36 (Figure 4).

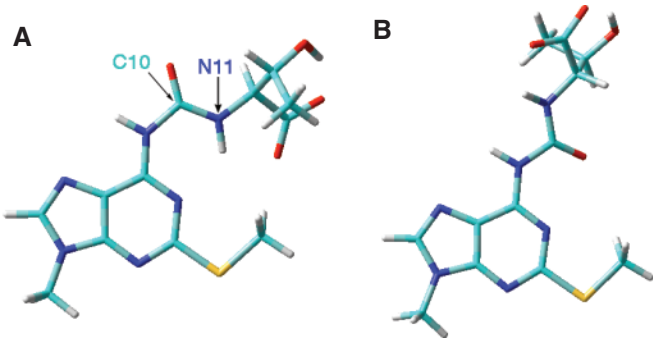

Figure 4. Conformations of ms^2t^6A. (**A**) with an ureido ring (**B**) without an ureido ring as calculated at the MPW1K/6-31+G (d,p) level of theory.

NMR studies indicate that the SCH_3 of ms^2t^6A weakens the ureido hydrogen-bonding interaction as compared to t^6A (29). Taken together with quantum calculations indicating facile interconversion at room temperature between an ureido ring conformation and a non-ureido ring structure, the conformation around C10-N11 may change based upon the context of the ribosome. In the *E.coli* 30S ribosomal subunit, primarily responsible for decoding (80), A1493, A1492 and G530 have been found to recognize the first two base pairs of the anticodon–codon complex in the minor groove (76), triggering a closure of the small subunit around the tRNA (81). In this system, the ureido ring allows greater stacking interactions with A38 (19), possibly giving U36 more flexibility to adjust to the codon. The prokaryotic and eukaryotic ribosomes contain conserved regions of rRNA around the decoding site (82) and mRNA crosslinks to A1493 and A1492 corresponding residues in human 18S subunits (83). However, human $tRNA^{Lys,3}$ may rotate the t^6 moiety around the C10-N11 bond allowing the t^6 side chain to hydrogen bond across the loop, thereby stabilizing U36 for correct positioning in the ribosome in a canonical fashion. Accuracy in tRNA–mRNA recognition is both dependent upon a kinetic proofreading mechanism and the stability of the cognate codon–anticodon complex (84). The role of modified bases in stablizing codon–anticodon complexes as opposed to destabilizing the loop conformation for an induced-fit in the ribosome seems to be base and system dependent (4).

SUPPLEMENTARY DATA

Supplementary Data are available at NAR Online.

ACKNOWLEDGEMENTS

The authors would like to thank Philippe Bénas for discussions on the structure of human $tRNA^{Lys,3}$. This work was supported by the Petroleum Research Fund (PRF 41701-GB7), the

National Science Foundation (DUE-0431664 and CHE-0521063) and Truman State University. Funding to pay the Open Access publication charges for this article was provided by the Petroleum Research Fund.

Conflict of interest statement. None declared.

REFERENCES

1. Limbach,P.A., Crain,P.F., Pomerantz,S.C. and McCloskey,J.A. (1995) Structures of posttranscriptionally modified nucleosides from RNA. *Biochimie*, **77**, 135–138.
2. Motorin,Y. and Grosjean,H. (1998) Appendix 1: chemical structures and classification of posttranscriptionally modified nucleosides in RNA. In Grosjean,H. and Benne,R. (eds), *Modification and Editing of RNA*. American Society for Microbiology Press, Washington, DC, pp. 534–549.
3. Yokoyama,S. and Nishimura,S. (1995) Modified nucleosides and codon recognition. In Soll,D. and RajBhandary,U.L. (eds), *tRNA: Structure, Biosynthesis and Function.* American Society for Microbiology, Washington, DC, pp. 207–223.
4. Agris,P.F. (2004) Decoding the genome: a modified view. *Nucleic Acids Res*., **32**, 223–238.
5. Sakurai,M., Ohtsuki,T. and Watanabe,K. (2005) Modification at position 9 with 1-methyladenosine is crucial for structure and function of nematode mitochondrial tRNAs lacking the entire T-arm. *Nucleic Acids Res*., **33**, 1653–1661.
6. Blaise,M., Becker,H.D., Keith,G., Cambillau,C., Lapointe,J., Giege,R. and Kern,D. (2004) A minimalist glutamyl-tRNA synthetase dedicated to aminoacylation of the tRNAAsp QUC anticodon. *Nucleic Acids Res*., **32**, 2768–2775.
7. Isel,C., Marquet,R., Keith,G., Ehresmann,C. and Ehresmann,B. (1993) Modified nucleotides of tRNA3lys modulate primer/template loop–loop interaction in the initiation complex of HIV-1 reverse transcription. *J. Biol. Chem*., **268**, 25269–25272.
8. Ashraf,S.S., Sochacka,E., Cain,R., Guenther,R., Malkiewicz,A. and Agris,P.F. (1999) Single atom modification (O→S) of tRNA confers ribosome binding. *RNA*, **5**, 188–194.
9. Yarian,C., Marszalek,M., Sochacka,E., Malkiewicz,A., Guenther,R., Miskiewicz,A. and Agris,P.F. (2000) Modified nucleoside dependent Watson–Crick and wobble codon binding by $tRNA^{Lys}_{UUU}$ species. *Biochemistry*, **39**, 13390–13395.
10. Phelps,S.S., Jeinic,O. and Joseph,S. (2002) Universally conserved interactions between the ribosome and the anticodon stem–loop of A site tRNA important for translocation. *Mol. Cell*, **10**, 799–807.
11. Phelps,S.S., Malkiewicz,A., Agris,P.F. and Joseph,S. (2004) Modified nucleotides in $tRNA^{Lys}$ and $tRNA^{Val}$ are important for translocation. *J. Mol. Biol*., **338**, 439–444.
12. Kruger,M., Pedersen,S. and Hagervall,T.G. (1998) The modification of the wobble base $tRNA^{Glu}$ modulates the translation rate of glutamic acid codons *in vivo*. *J. Mol. Biol*., **284**, 621–631.
13. Brierley,I., Meredith,M.R., Bloys,A.J. and Hagervall,T.G. (1997) Expression of a coronavirus ribosomal frameshift signal in *Escherichia coli*: influence of tRNA anticodon modification on frameshifting. *J. Mol. Biol*., **270**, 360–373.
14. Sprinzl,M. and Vassilenko,K.S. (2005) Compilation of tRNA sequences and sequences of tRNA genes. *Nucleic Acids Res*., **33**, D139–D149.
15. Bjork,G.R. (1995) Biosynthesis and function of modified nucleosides. In Söll,D. and RajBhandary,U.L. (eds), *tRNA: Structure, Biosynthesis, and Function*. American Society for Microbiology Press, Washington, DC, pp. 165–206.
16. Agris,P.F. (1996) The importance of being modified: roles of modified nucleosides and Mg^{2+} in RNA structure and function. *Prog. Nucleic Acid Res. Mol. Biol*., **53**, 79–129.
17. Davis,D.R., Veltri,C.A. and Nielsen,L. (1998) An RNA model system for investigation of pseudouridine stabilization of the codon–anticodon interaction in $tRNA^{Lys}$, $tRNA^{His}$ and $tRNA^{Tyr}$. *J. Biomol. Struct. Dyn*., **15**, 1121–1132.
18. Durant,P.C. and Davis,D.R. (1999) Stabilization of the anticodon stem–loop of $tRNA^{Lys,3}$ by an A^{+}–C base pair and by pseudouridine. *J. Mol. Biol*., **285**, 115–131.
19. Murphy,F.V., Ramakrishnan,V., Malkiewicz,A. and Agris,P.F. (2004) The role of modifications in codon discrimination by $tRNA^{Lys}_{UUU}$. *Nature Struct. Mol. Biol*, **11**, 1186–1191.
20. Chen,Y., Sierzputowska-Gracz,H., Guenther,R., Everett,K. and Agris,P.F. (1993) 5-Methylcytidine is required for cooperative binding of magnesium(2+) and a conformational transition at the anticodon stem–loop of yeast phenylalanine tRNA. *Biochemistry*, **32**, 10249–10253.
21. Nobles,K.N., Yarian,C.S., Liu,G., Guenther,R.H. and Agris,P.F. (2002) Highly conserved modified nucleosides influence Mg^{2+}-dependent tRNA folding. *Nucleic Acids Res*., **30**, 4751–1760.
22. Cabello-Villegas,J., Tworowska,I. and Nikonowicz,E.P. (2004) Metal ion stabilization of the U-turn of the A_{37} N^{6}-dimethylallyl-modified anticodon stem–loop of *Escherichia coli* $tRNA^{Phe}$. *Biochemistry*, **43**, 55–66.
23. Von Ahsen,U., Green,R., Schroeder,R. and Noller,H.F. (1997) Identification of 2-hydroxyl groups required for interaction of a tRNA anticodon stem–loop region with the ribosome. *RNA*, **3**, 49–56.
24. Lustig,F., Elias,P., Axberg,T., Samuelsson,T., Tittawella,I. and Lagerkvist,U. (1981) Codon reading and translational error. *J. Biol. Chem*., **256**, 2635–2643.
25. Yarian,C., Townsend,H., Czestkowski,W., Sochacka,E., Malkiewicz,A., Guenther,R., Miskiewicz,A. and Agris,P.F. (2002) Accurate translation of the genetic code depends on tRNA modified nucleosides. *J. Biol. Chem*., **227**, 16391–16395.
26. Durant,P.C. and Davis,D.R. (1997) The effects of pseudouridine and pH on the structure and dynamics of the anticodon stem–loop of $tRNA^{Lys,3}$. *Nucleic Acids Symp. Ser*., **36**, 56–57.
27. Stuart,J.W., Gdaniec,Z., Guenther,R., Marszalek,M., Sochacka,E., Malkiewicz,A. and Agris,P.F. (2000) Functional anticodon architecture of human $tRNA^{Lys3}$ includes disruption of intraloop hydrogen bonding by the naturally occurring amino acid modification, $t^{6}A$. *Biochemistry*, **39**, 13396–13404.
28. Sundaram,M., Durant,P.C. and Davis,D.R. (2000) Hypermodified nucleosides in the anticodon of $tRNA^{Lys}$ stabilize a canonical U-turn structure. *Biochemistry*, **39**, 12575–12584.
29. Durant,P.C., Baji,A.C., Sundaram,M., Kumar,R.K. and Davis,D.R. (2005) Structural effects of hypermodified nucleosides in the *Escherichia coli* and human $tRNA^{Lys}$ anticodon loop: the effect of nucleosides $s^{2}U$, $mcm^{5}U$, $mcm^{5}s^{2}U$, $mnm^{5}s^{2}U$, $t^{6}A$, and $ms^{2}t^{6}A$. *Biochemistry*, **44**, 8078–8089.
30. Bénas,P., Bec,G., Keith,G., Marquet,R., Ehresmann,C., Ehresmann,B. and Dumas,P. (2000) The crystal structure of HIV reverse-transcription primer $tRNA^{Lys,3}$ shows a canonical anticodon loop. *RNA*, **6**, 1347–1355.
31. Fuller,W. and Hodgson,A. (1967) Conformation of the anticodon loop in tRNA. *Nature*, **215**, 817–821.
32. Grosjean,H. and Benne,R. (1998) *Modification and Editing of RNA*. American Society for Microbiology Press, Washington, DC.
33. Cornell,W.D., Cieplak,P., Bayly,C.I., Gould,I.R., Merz,K.M., Jr, Ferguson,D.M., Spellmeyer,D.C., Fox,T., Caldwell,J.W. and Kollman,P.A. (1995) A second generation force field for the simulation of proteins, nucleic acids, and organic molecules. *J. Am. Chem. Soc*., **117**, 5179–5197.
34. Case,D.A., Pearlman,D.A., Caldwell,J.W., Cheatham,T.E., III, Ross,W.S., Simmerling,C.L., Darden,T.A., Mertz,K.M., Stanton,R.V., Cheng,A.L. *et al*. (1999) 6.0 edn. University of California, San Francisco, CA.
35. Jorgensen,W.L., Chandrasekhar,J. and Madura,J.D. (1983) Comparison of simple potential functions for simulating liquid water. *J. Chem. Phys*., **79**, 926–935.
36. York,D.M., Darden,T.A. and Pedersen,L.G. (1993) The effect of long-range electrostatic interactions in simulations of macromolecular crystals: a comparison of the Ewald and truncated list methods. *J. Chem. Phys*., **99**, 8345–8348.
37. Ryckaert,J.P., Ciccotti,G. and Berendsen,H.J.C. (1977) Numerical integration of the Cartesian equations of motion of a systems with constraints: molecular dynamics of *n*-alkanes. *J. Comput. Phys*., **23**, 327–341.
38. Berendsen,H.J.C., Postma,J.P.M., van Gunsteren,W.F., A. DiNola,A. and Haak,J.R. (1984) Molecular dynamics with coupling to an external bath. *J. Comput. Phys*., **81**, 3684–3690.
39. Cheatham,T.E., III and Kollman,P.A. (1997) Molecular dynamics simulations highlight the structural differences among DNA:DNA, RNA:RNA, and DNA:RNA hybrid duplexes. *J. Am. Chem. Soc*., **119**, 4805–4825.

40. Auffinger,P., Bielecki,L. and Westhof,E. (2004) Symmetric K^+ and Mg^{2+} ion-binding sites in the 5S rRNA loop E inferred from molecular dynamics simulations. *J. Mol. Biol.*, **335**, 555–571.
41. Auffinger,P. and Westhof,E. (1997) RNA hydration: three nanoseconds of multiple molecular dynamics simulations of the solvated $tRAN^{Asp}$ anticodon hairpin. *J. Mol. Biol.*, **269**, 326–341.
42. Dixit,S.B., Beveridge,D.L., Case,D.A., Cheatham,T.E., III, Giudice,E., Lankas,F., Lavery,R., Maddocks,J.H., Osman,R., Sklenar,H. *et al.* (2005) Molecular dynamics simulations of the 136 unique tetranucleotide sequences of DNA oligonucleotides. II: sequence context effects on the dynamical structures of the 10 unique dinucleotide steps. *Biophys. J.*, **89**, 3721–3740.
43. Mokdad,A., Krasovska,M.V., Sponer,J. and Leontis,N.B. (2006) Structural and evolutionary classification of G/U wobble basepairs in the ribosome. *Nucleic Acids Res.*, **34**, 1326–1341.
44. Nagan,M.C., Kerimo,S.S., Musier-Forsyth,K. and Cramer,C.J. (1999) Wild-type RNA $microhelix^{Ala}$ and 3:70 variants: molecular dynamics analysis of local helical structure and tightly bound water. *J. Am. Chem. Soc.*, **121**, 7310–7317.
45. Spackova,N. and Sponer,J. (2006) Molecular dynamics simulations of sarcin–ricin rRNA motif. *Nucleic Acids Res.*, **34**, 697–708.
46. Wang,J., Wolf,R.M., Caldwell,J.W., Kollman,P.A. and Case,D.A. (2003) Development and testing of a general amber force field. *J. Comput. Chem.*, **25**, 1157–1174.
47. Hehre,W.J., Radom,L., Schleyer,P.v.R. and Pople,J.A. (1986) *Ab Initio Molecular Orbital Theory*. Wiley, NY.
48. Ditchfield,R., Hehre,W.J. and Pople,J.A. (1971) Self-consistent molecular-orbital methods. IX. An extended Gaussian-type basis for molecular-orbital studies of organic molecules. *J. Chem. Phys.*, **54**, 724–728.
49. Hariharan,P.C. and Pople,J.A. (1972) The effects of d-functions on molecular orbital energies for hydrocarbons. *Chem. Phys. Lett.*, **66**, 217–219.
50. Hehre,W.J., Ditchfield,R. and Pople,J.A. (1972) Self-consistent molecular orbital methods. XII. Further extensions of Gaussian-type basis sets for use in molecular orbital studies of organic molecules. *J. Am. Chem. Soc.*, **56**, 2257–2261.
51. Bayly,C.I., Cieplak,P., Cornell,W.D. and Kollman,P.A. (1993) A well-behaved electrostatic potential based method using charge restraints for determining atom-centered charges: the RESP model. *J. Phys. Chem.*, **97**, 10269–10280.
52. Frisch,M.J., Trucks,G.W., Schlegel,H.B., Scuseria,G.E., Robb,M.A., Cheeseman,J.R., Montgomery,J.J.A., Vreven,T., Kudin,K.N., Burant,J.C. *et al.* (2003) Revision B.04 ed. Gaussian, Inc., Wallingsford, CT.
53. Lynch,B.J., Fast,P.L., Harris,M. and Truhlar,D.G. (2000) Adiabatic connection for kinetics. *J. Phys. Chem. A*, **104**, 4811–4815.
54. Lynch,B.J., Zhao,Y. and Truhlar,D.G. (2003) Effectiveness of diffuse basis functions for calculating relative energies by density functional theory. *J. Phys. Chem. A*, **107**, 1384–1388.
55. Hariharan,P.C. and Pople,J.A. (1973) Influence of polarization functions on MO hydrogenation energies. *Theor. Chim. Acta*, **28**, 213–222.
56. Francl,M.M., Pietro,W.J., Hehre,W.J., Binkley,J.S., Gordon,M.S., DeFrees,D.J. and Pople,J.A. (1982) Self-consistent molecular orbital methods. XXIII. A polarization-type basis set for second-row elements. *J. Chem. Phys.*, **77**, 3654–3665.
57. Lu,X. and Olson,W.K. (2003) 3DNA: a software package for the analysis, rebuilding and visualization of three-dimensional nucleic acid structures. *Nucleic Acids Res.*, **31**, 5108–5121.
58. Humphrey,W., Dalke,A. and Schulten,K. (1996) VMD: visual molecular dynamics. *J. Mol. Graph*, **14**, 33–38.
59. Pettersen,E.F., Goddard,T.D., Huang,C.C., Couch,G.S., Greenblatt,D.M., Meng,E.C. and Ferrin,T.E. (2004) UCSF Chimera—a visualization system for exploratory research and analysis. *J. Comput. Chem.*, **25**, 1605–1612.
60. Connolly,M.L. (1983) Analytical molecular surface calculation. *J. Appl. Cryst.*, **16**, 548–558.
61. Case,D.A., Darden,T.A., Cheatham,T.E., III, Simmerling,C.L., Wang,J., Duke,R.E., Luo,R., Merz,K.M., Wang,B., Pearlman,D.A. *et al.* (2004) Scripps Research Institute, La Jolla, CA.
62. Lavery,R. and Zakrzewska,K. (1999) Base and base pair morphologies, helical parameters, and definitions. In Neidle,S. (ed.), *Oxford Handbook of Nucleic Acid Structure*. Oxford University Press, NY, pp. 39–76.
63. Olson,W.K. and Dasika,R.D. (1976) Spatial configuration of ordered polynucleotide chains. 3. Polycyclonucleotides. *J. Am. Chem. Soc.*, **98**, 5371–5380.
64. Nagan,M.C., Beuning,P., Musier-Forsyth,K. and Cramer,C.J. (2000) Importance of discriminator base stacking interactions: molecular dynamics analysis of A73 $microhelix^{Ala}$ variants. *Nucleic Acids Res.*, **28**, 2527–2534.
65. Parthasarathy,R., Ohrt,J.M. and Chheda,G.B. (1977) Modified nucleosides and conformation of anticodon loops: crystal structure of t^6A and g^6A. *Biochemistry*, **16**, 4999–5008.
66. Cabello-Villegas,J., Winkler,M.E. and Nikonowicz,E.P. (2002) Solution conformations of unmodified and $A_{37}N^6$-dimethylallyl modified anticodon stem–loops of *Escherichia coli* $tRNA^{Phe}$. *J. Mol. Biol.*, **319**, 1015–1034.
67. Auffinger,P. and Westhof,E. (1998) Effects of pseudouridylation. In Grosjean,H. and Benne,R. (eds), *Modification and Editing of RNA*. ASM Press, Washington, DC, pp. 103–112.
68. Westhof,E., Dumas,P. and Moras,D. (1988) Hydration of transfer RNA molecules: a crystallographic study. *Biochimie*, **70**, 145–165.
69. Griffey,R.H., Davis,D.R., Yamaizumi,Z., Nishimura,S., Bax,A., Hawkins,B. and Poulter,C.D. (1985) ^{15}N-labeled *Escherichia coli* $tRNA_f^{Met}$, $tRNA^{Glu}$, $tRNA^{Tyr}$, and $tRNA^{Phe}$. *J. Biol. Chem.*, **260**, 9734–9741.
70. Davis,D.R. and Poulter,C.D. (1991) ^1H-^{15}N NMR studies of *Escherichia coli* $tRNA^{Phe}$ from hisT mutants: a structural role for pseudouridine. *Biochemistry*, **30**, 4223–4231.
71. Zacharias,M. and Skelnar,H. (1999) Conformational analysis of single-base bulges in A-form DNA and RNA using a hierarchical approach and energetic evaluation with a continuum solvent model. *J. Mol. Biol.*, **289**, 261–275.
72. Ladner,J.E., Jack,A., Robertus,J.D., Brown,R.S., Rhodes,D., Clark,B.F.C. and Klug,A. (1975) A structure of yeast phenylalanine transfer RNA at 2.5 Å resolution. *Proc. Natl Acad. Sci. USA*, **72**, 4414–4418.
73. Westhof,E., Dumas,P. and Moras,D. (1985) Crystallographic refinement of yeast aspartic acid transfer RNA. *J. Mol. Biol.*, **194**, 119–145.
74. Moras,D., Dock,A.C., Dumas,P., Westhof,E., Romby,P., Ebel,J.P. and Giege,R. (1986) Anticodon-anticodon interaction induces conformational changes in tRNA: yeast $tRNA^{Asp}$, a model for tRNA–mRNA recognition. *Proc. Natl Acad. Sci. USA*, **83**, 932–936.
75. Basavappa,R. and Sigler,P.B. (1991) The 3 Å crystal structure of yeast initiator tRNA: functional implications in initiator/elongator discrimination. *EMBO J.*, **10**, 2105–3111.
76. Ogle,J.M., Brodersen,D.E., Clemons,W.M., Tarry,M.J., Carter,A.P. and Ramakrishnan,V. (2001) Recognition of cognate transfer RNA by the 30S ribosomal unit. *Science*, **292**, 897–902.
77. Guckian,K.M., Ren,R.X.-F., Chaudhuri,N.C., Tahmassebi,D.T. and Kool,E.T. (2000) Factors contributing to aromatic stacking in water: evaluation in the context of DNA. *J. Am. Chem. Soc.*, **122**, 2213–2222.
78. Kool,E.T. (2002) Replacing the nucleobases in DNA with designer molecules. *Acc. Chem. Res.*, **35**, 936–943.
79. Fredericks,S.Y., Jorda,K.D. and Zwier,T.S. (1996) Theoretical characterization of the structures and vibrational spectra of benzene-$(H_2O)_n$ ($n = 1$–3) clusters. *J. Phys. Chem.*, **100**, 7810–7821.
80. Carter,A.P., Clemons,W.M., Jr, Brodersen,D.E., Morgan-Warren,R.J., Wimberly,B.T. and Ramakrishnan,V. (2000) Functional insights from the structure of the 30S ribosomal subunit and its interactions with antibiotics. *Nature*, **407**, 340–348.
81. Ogle,J.M., Murphy,F.V., IV, Tarry,M.J. and Ramakrishnan,V. (2002) Selection of tRNA by the ribosome requires a transition from an open to a closed form. *Cell*, **111**, 721–732.
82. Spahn,C.M.T., Beckmann,R., Eswar,N., Penczek,P.A., Sali,A., Blobel,G. and Frank,J. (2001) Structure of the 80S ribosome from *Saccharomyces cerevisiae*–tRNA–ribosome and subunit–subunit interactions. *Cell*, **107**, 373–386.
83. Graifer,D., Molotkov,M., Styazhkina,V., Demeshkina,N., Bulygin,K., Eremina,A., Ivanov,A., Laletina,E., Ven'Yaminova,A. and Karpova,G. (2004) Variable and conserved elements of human ribosomes surrounding the mRNA at the decoding and upstream sites. *Nucleic Acids Res.*, **32**, 3282–3293.
84. Rodnina,M.V. and Wintermeyer,W. (2001) Ribosome fidelity: tRNA discrimination, proofreading and induced fit. *TIBS*, **26**, 124–130.